Research Square

Preprints are preliminary reports that have not undergone peer review.
They should not be considered conclusive, used to inform clinical practice,
or referenced by the media as validated information.

Macrophage-Biomimetic Porous Se@SiO_2 Nanocomposites For “Dual Model” Immunotherapy Against Inflammatory Osteolysis

Cheng Ding
Shanghai 6th Peoples Hospital Affiliated to Shanghai Jiaotong University School of Medicine
Chuang Yang
Shanghai 6th Peoples Hospital Affiliated to Shanghai Jiaotong University School of Medicine
Tao Cheng
Shanghai 6th Peoples Hospital Affiliated to Shanghai Jiaotong University School of Medicine
Xingyan Wang
Shanghai University of Engineering Science
Qiaojie Wang
Shanghai 6th Peoples Hospital Affiliated to Shanghai Jiaotong University School of Medicine
Renke He
Shanghai 6th Peoples Hospital Affiliated to Shanghai Jiaotong University School of Medicine
Shang Sang
Shanghai 6th Peoples Hospital Affiliated to Shanghai Jiaotong University School of Medicine
Kechao Zhu
Shanghai 6th Peoples Hospital Affiliated to Shanghai Jiaotong University School of Medicine
Dongdong Xu
Shanghai 6th Peoples Hospital Affiliated to Shanghai Jiaotong University School of Medicine
Jiaxing Wang
Shanghai 6th Peoples Hospital Affiliated to Shanghai Jiaotong University School of Medicine
Xijian Liu
Shanghai University of Engineering Science
Xianlong Zhang (✉ dr_zhangxianlong@163.com)
Shanghai Jiao Tong University Affiliated Sixth People's Hospital https://orcid.org/0000-0003-2122-9990

Research

Keywords: biomimetic nanoparticle, porous Se@SiO2 nanospheres, macrophage polarization, osteolysis, immunomodulation

Posted Date: September 21st, 2021

DOI: https://doi.org/10.21203/rs.3.rs-885656/v1

License: This work is licensed under a Creative Commons Attribution 4.0 International License.
Read Full License

Abstract

Background Inflammatory osteolysis is a major complication of total joint replacement surgery that can cause prosthesis failure and necessitate revision surgery. Macrophages are key effector immune cells in inflammatory responses, but excessive M1-polarization of dysfunctional macrophages leads to the secretion of pro-inflammatory cytokines and severe loss of bone tissue. Here, we report the development of macrophage-biomimetic porous SiO_2-coated ultrasmall Se particles (Porous Se@SiO_2 nanospheres) for the management of inflammatory osteolysis.

Results: Macrophage-membrane-coated porous Se@SiO_2 nanospheres(M-Se@SiO_2) can attenuate lipopolysaccharide (LPS)-induced inflammatory osteolysis by a dual-immunomodulatory effect. As macrophage membrane decoys, these nanoparticles reduce toxin levels and neutralize pro-inflammatory cytokines. Moreover, the release of Se can induce the polarization of macrophages toward the anti-inflammatory M2-phenotype. These effects are mediated via the inhibition of p65, p38, and extracellular signal-regulated kinase(ERK) signaling. Additionally, the immune environment created by M-Se@SiO_2 reduces the inhibition of osteogenic differentiation caused by pro-inflammation cytokines, confirmed through *in vitro* and *in vivo* experiments.

Conclusion: Our findings suggest that M-Se@SiO_2 has an immunomodulatory role in LPS-induced inflammation and bone remodeling, which demonstrates that M-Se@SiO_2 is a promising engineered nano-platform for the treatment of osteolysis arising after arthroplasty.

Background

For end-stage diseases that affect joints, total joint replacement is the most common and successful surgical treatment method. However, following replacement therapy, aseptic loosening and periprosthetic joint infection are serious complications that can cause inflammatory osteolysis, affecting the continued use of prosthesis, resulting in the need for revision surgery and posing a heavy economic burden.[1, 2] Inflammatory osteolysis is induced by bacterial products and/or implant-derived wear particles, which activate innate immune cells to produce pro-inflammatory factors that can disrupt osteogenic processes and destruct bone.[3–5]

Macrophages are key effector immune cells in inflammatory osteolysis and are generally considered to have two polarization states following activation, namely M1- and M2-phenotypes. Following exposure to certain inflammatory stimuli, excessive polarization of macrophages toward a pro-inflammatory M1 phenotype is accompanied by the secretion of large amounts of pro-inflammatory cytokines such as interleukin (IL)-6 and tumor necrosis factor-alpha (TNF-α), which enhance osteoclasts activity and impair the osteogenic process.[6, 7] In contrast, M2-type macrophages are induced by IL-4 or transforming growth factor-beta, and then, they secrete IL-10 and IL-4 to inhibit inflammation and promote tissue repair and functional recovery.[8, 9] Several studies have demonstrated that M2 macrophages have important roles in bone immunology and that an appropriate anti-inflammatory immune response attenuates bone

tissue damage while facilitating the osteogenic process.[10–12] Hence, avoiding excessive M1-polarization and promoting M2-polarization are critical for reducing bone tissue loss and promoting repair. Se is an essential trace element for the human body, as it plays a key role in nutrition, physiology, pathology, and disorder treatments.[13] Studies have shown that it has anti-oxidative, anti-inflammatory, and regulatory functions in immune cells.[14–16] Moreover, Se can regulate macrophage phenotypes and improve the anti-inflammatory ability of macrophages to promote tissue repair and cell proliferation.[17] However, its relatively narrow range between effective concentration and toxicity limits the application of Se-containing drugs.[18] Hence, we previously developed porous SiO_2-coated ultrasmall Se particles (Se@SiO_2 nanospheres) for drug delivery, which slowly release effective Se at effective concentrations, thereby reducing toxicity and improving biocompatibility.[19]

Lipopolysaccharide (LPS), an endotoxin derived from the cell wall of gram-negative bacteria, is an effective inducer of immune cells and a key factor in the occurrence of inflammatory osteolysis.[20, 21] LPS promotes M1 polarization through the membrane-bound toll-like receptor 4 (TLR4) and its downstream nuclear factor-κB (NF-κB) and p38 mitogen-activated protein kinase (MAPK) signaling pathways, resulting in the secretion of pro-inflammatory cytokines.[22] In recent years, engineered nanoparticles coated with cell membranes have increasingly been used in cancer treatment, disease diagnosis, antibacterial activity, and detoxification.[23–26] Cell membrane-based nano-platforms are characterized by evasion of phagocytosis, prolonged circulation life, and targeted therapy.[27–29] Moreover, cell membranes of various cells such as red blood cells, macrophages, platelets, and tumor cells can be used according to different functional requirements.[30–32] For instance, macrophage-membrane-coated nanoparticles have been used for the treatment of sepsis, rheumatoid arthritis and bone regeneration due to their ability to neutralize endotoxins and proinflammatory cytokines, providing a promising delivery system of nanotherapeutics against inflammatory osteolysis.[33–35] Macrophage-membrane-coated nanoparticles exhibit the same characteristics antigenic properties as macrophages and their membrane protein receptors are conserved, indicating their potential to bind to inflammatory mediators and block inflammatory responses. In light of the above findings, reducing the production of inflammatory stimuli and regulating macrophage polarization are two potentially curative approaches to inhibit osteolysis.

In this study, we established a macrophage-membrane-coated porous Se@SiO2 nanospheres(M-Se@SiO_2) drug delivery system. Macrophage membranes express key protein receptors such as TNF-R, IL6-R, and TLR4, binding to inflammatory cytokines TNF-α, IL-6, and endotoxin LPS to inhibit M1-polarization. Simultaneously, porous Se@SiO_2 nanospheres release Se to induce the polarization of macrophages toward the anti-inflammatory M2-phenotype, thereby reducing excessive pro-inflammatory activity and promoting osteogenesis. These effects may be mediated via the inhibition of p65, p38, and extracellular signal-regulated kinase signaling. Additionally, the immunomodulatory effect of macrophages on osteogenic differentiation was investigated. M-Se@SiO2 reduced the inhibition of osteogenic differentiation caused by inflammation cytokines. This study provides a dual-immunomodulatory strategy for the treatment of inflammatory osteolysis. The biomimetic membrane

system reduces toxin levels and neutralizes inflammatory cytokines, and selenium released from nanoparticles regulates the polarization of macrophages. The findings showed that M-Se@SiO2 may serve as a new tool for immunomodulatory osteogenesis in the microenvironment.

Results And Discussion

Characterization of M-Se@SiO_2

M-Se@SiO_2 is composed of the macrophage membrane loaded onto the surface of porous Se@SiO_2 nanospheres. After synthesizing porous Se@SiO_2 nanospheres according to a previously described method[36] and isolating membrane vesicles of macrophage cells, the membrane vesicles were polymerized onto porous Se@SiO_2 nanospheres (Fig. 1A). Transmission electron microscopy (TEM) images of the Se@SiO_2 nanospheres showed abundant Se nanoparticles interspersed in the silica shell (Fig. 1B). Moreover, Se@SiO_2 nanospheres formed porous structures after immersion in the water (Fig. 1C). X-ray diffractometry (XRD) patterns of Se@SiO_2 nanospheres correspond well with the diffraction peaks of standard Se and showed the silica peak at ~ 23^o (Fig. 1D), confirming the successful synthesis of Se@SiO_2. M-Se@SiO_2 particles were subsequently dyed with phosphotungstic acid and examined using TEM. The nanoparticles showed a thin uniform coating on the surface (Fig. 1E, F). Moreover, the zeta potential of the membrane surface decreased from − 21.30 ± 1.61 to − 48.27 ± 2.34 mV, which is similar to that of macrophage membrane vesicles. There were no obvious changes in the hydrodynamic size of M-Se@SiO_2 after 72 h (Fig. 1G), showing good colloidal stability. Due to the porous structure, Se could be continuously released from M-Se@SiO_2 and porous Se@SiO_2 (Fig. 1H), thus confirming good biocompatibility and long-term treatment effect. After membrane fusion, the diameter of the nanoparticles increased from ~ 73 to ~ 98 nm as measured by dynamic light scattering (DLS), which corresponded to a macrophage membrane of approximately 10 nm on porous Se@SiO_2 nanospheres (Fig. 1I). In addition, western blotting was used to analyze key proteins on the membrane surface. The TLR4 receptor is the main protein that binds to endotoxin, whereas IL6-R and TNFR bind to the pro-inflammatory factors IL-6 and TNF-α, respectively (Fig. 1J). These receptors were expressed on the macrophage membrane and exhibited strong binding potential. Furthermore, the ability of M-Se@SiO_2 to bind LPS and the pro-inflammatory cytokines TNF-α and IL-6 was investigated. Solutions containing LPS-FITC, or cytokines were incubated with M-Se@SiO_2 nanospheres for 30 min, and the LPS or cytokine concentrations were measured thereafter. M-Se@SiO_2 nanospheres effectively removed LPS, IL-6, and TNF-α, demonstrating that M-Se@SiO_2 can effectively bind to LPS and pro-inflammatory cytokines (Fig. 1K). In summary, these results indicate that porous Se@SiO_2 nanospheres were successfully modified with macrophage membranes that retained key proteins, thereby enhancing drug delivery, reducing toxin levels, and neutralizing inflammatory factors. The membranes used to coat nanospheres can play different roles depending on their cell of origin; for instance, erythrocytes with good immune evasion prolong the duration of nanosphere circulation, thereby extending the delivery of anti-infection drugs.[23] Meanwhile, tumor cells increase the homologous recognition for anti-tumor therapy,[24] and

macrophages and neutrophils reduce immune system clearance while adsorbing endotoxins and cytokines to reduce inflammation.[33, 37] Indeed, platelet, bacterial, and mitochondrial membranes are increasingly used to coat nanospheres.[31, 38, 39] Moreover, the inner layer of porous Se@SiO_2 nanospheres suppresses inflammation by releasing ultramicroscopic quantum dots of Se. Silica platforms are excellent nanocarriers due to their high biocompatibility, controlled drug loading, and simple production.[19] Se, a trace element that regulates immune functions, has anti-oxidative properties, and promotes bone formation.[40–42] A study in a urethral wound healing model reported that porous Se@SiO_2 nanospheres could regulate macrophage functions.[43] As expected, in the present study, M-Se@SiO_2 inhibited LPS-induced osteolysis by both adsorption of pro-inflammatory mediators and regulation of macrophage polarization.

We used the Cell Counting Kit 8(CCK-8) assay to evaluate the cytotoxicity of porous Se@SiO_2 nanospheres and M-Se@SiO_2 with respect to murine bone marrow-derived macrophages (BMDMs) and bone mesenchymal stem cell (BMSCs). Porous Se@SiO_2 nanospheres did not show significant cytotoxicity up to 10 μg/mL. However, concentrations exceeding 10 μg/mL led to concentration-dependent cytotoxicity. Similarly, no significant cytotoxicity was detected after treatment with M-Se@SiO_2 up to 10 μg/mL (Fig. 1L).

In vitro **evaluation of macrophage polarization**

Inflammatory osteolysis caused by bacterial products or wear particles leads to bone loss near prosthesis. This is a major cause of failure of joint replacement surgery.[4, 44] Macrophages are important immune cells that play a key role in osteolysis and are important targets of bone remodeling. Different polarization states of macrophages have distinct functions and can be influenced by specific external factors. The M1-type macrophages express effector molecules such as inducible nitric oxide synthase (iNOS), upregulate surface molecules such as CD86 and C-C chemokine receptor type 7 (CCR7), and secret pro-inflammatory cytokines including interleukin (IL)-6 and tumor necrosis factor-alpha (TNF-α), which lead to inflammatory processes in osteolysis[6]. In contrast, M2-type macrophages, secrete anti-inflammatory factors IL-10 and IL-4 and express effector molecules such as arginase 1 (ARG1) and surface molecules such as CD206 and CD163 to inhibit inflammation and promote osteogenic differentiation and tissue regeneration.[45]

To identify macrophage phenotypes, we used flow cytometry to quantify the proportion of M1- and M2-type macrophages by evaluating the expression levels of CCR7 and CD206, surface markers for M1 and M2 phenotypes, respectively (Fig. 2A, 2B, 2C, and 2D). The percentage of CCR7-positive cells increased from 15.9% in the control group to 29.8% in the LPS-treated group. In contrast, CCR7 positivity decreased to 21.4% after M-Se@SiO_2 treatment, which was lower than that in the Se@SiO_2-treated group (24.9%). The percentage of M2 cells expressing the surface marker CD206 showed the following trend: control (15.9%) < LPS (24.1%) < LPS + Se@SiO_2 (33.3%) < LPS + M-Se@SiO_2 (38.5%). To investigate whether M-Se@SiO_2 has the ability to regulate M1/M2 polarization of BMDMs, we selected representative genes and

assessed their expression using quantitative real-time polymerase chain reaction (RT-PCR) (Fig. 2E). The M1-associated genes *CD86* and *iNOS* were substantially downregulated in LPS-stimulated cultures treated with M-Se@SiO_2 compared with those in only LPS-stimulated cultures, whereas the M2-associated genes *CD206* and *Arg1* were upregulated. Meanwhile, the osteoblast cytokine gene bone morphogenetic protein-2 (*BMP-2*) was upregulated in the LPS + M-Se@SiO_2-treated group compared with that in the LPS-treated group. This suggests a role for M-Se@SiO_2 in the immunomodulation of osteogenesis and inhibition of inflammation. To further detect representative cytokines secreted by M1 and M2 macrophages, the concentrations of TNF-α, IL-6, IL-4, and IL-10 were measured using enzyme-linked immunosorbent assay (ELISA) (Fig. 2F). Cells treated with LPS + M-Se@SiO_2 secreted more anti-inflammatory cytokines IL-4 and IL-10, which are mainly produced by M2 macrophages, than LPS- and LPS + Se@SiO_2-treated macrophages. Moreover, macrophages treated with LPS + M-Se@SiO_2 secreted less TNF-α and IL-6, pro-inflammatory factors produced by M1 cells, than the LPS-treated group. Thus, the ELISA and PCR results were in agreement. The expression of the M1marker CCR7 (Alexa Fluor 488, green) and M2 marker ARG-1 (Alexa Fluor 594, red) in BMDMs was detected by immunofluorescence staining. The LPS + M-Se@SiO_2 group exhibited fewer CCR7-positive cells than the LPS and LPS + Se@SiO_2 groups. In contrast, the expression of ARG-1 was higher in the LPS + M-Se@SiO_2 group than in other groups. (Fig. 3)

M-Se@SiO_2 attenuates LPS-induced activation of p65, ERK, and p38 phosphorylation in vitro

LPS stimulation promotes M1 polarization via the TLR4 pathway. Generally, TLR4 mediates LPS stimulation downstream of the p38 mitogen-activated protein kinase (MAPK) signaling pathway and nuclear factor-κB (NF-κB) signaling pathway.[46] The NF-κB pathway is important for macrophage polarization. NF-κB is composed of homodimers or heterodimers (p65, p50) that bind in their inactive state to IκB in the cytoplasm. Once activated, NF-κB p65 separates from IκB and translocates to the nucleus, where it binds to the promoters of its target genes.[47] The MAPK pathway is also a key pathway for macrophage polarization and inflammation, involving the ERK, p38, and c-Jun N-terminal kinase (JNK) subfamilies. Activation of the ERK, p38, and JNK pathways in response to LPS stimulation phosphorylates these proteins and promotes the expression of pro-inflammatory factors. Therefore, both NF-κB and MAPK are ideal targets for anti-inflammatory drugs.[22] Moreover, Se can inhibit the MAPK and NF-κB pathways, thereby exerting anti-inflammatory effects.[48] To investigate the effects of M-Se@SiO_2 treatment on the LPS-stimulated NF-κB pathway, the abundance of p65 was examined. Significant inhibition of LPS-induced p65 phosphorylation was observed after M-Se@SiO_2 administration. LPS also activates the MAPK pathway and drives M1 macrophage polarization. In the present study, LPS promoted the phosphorylation of p38 and ERK, whereas M-Se@SiO_2 treatment inhibited their phosphorylation (Fig. 4). Taken together, our results suggest that M-Se@SiO_2 inhibits LPS-induced polarization of M1 macrophages through the MAPK/NF-κB signaling pathways.

Osteogenic differentiation ability of BMDM-conditioned medium

Previous studies have shown that macrophages play a central regulatory role in all phases of bone regeneration and that cytokines contribute to this effect.[12] Therefore, we prepared conditioned media by collecting macrophage culture supernatants to observe their effects on the osteogenic process. BMDM cell culture supernatant was used as a conditioned medium to assess its effects on the osteogenic differentiation of BMSCs. The results of alkaline phosphatase (ALP) and alizarin red (ARS) staining are shown in Fig. 5A and 5B. ALP and ARS staining was weaker in the LPS group than in the control group, indicating the inhibition of osteogenic differentiation. In contrast, these staining intensities were higher in the LPS + M-Se@SiO_2 group than in the LPS + Se@SiO_2 and LPS groups. Quantification of ALP and ARS activities revealed similar results (Fig. 5C and 5D). We also examined the expression of three crucial genes related to osteogenesis, *BMP*-2, osteocalcin (*OCN*), and osteopontin (*OPN*) by RT-PCR. All genes were downregulated following incubation with LPS-conditioned medium compared with that in the control group. Meanwhile, the LPS + M-Se@SiO_2 group presented higher mRNA expression of these three genes than the LPS and LPS + Se@SiO_2 groups (Fig. 5E). These findings indicate that the osteogenic process was significantly inhibited in the presence of conditioned medium after LPS stimulation, whereas osteogenic differentiation was upregulated after M-Se@SiO_2 treatment compared with LPS and LPS + Se@SiO_2 groups.

In vivo **air pouch and cranial bone model.**

The air pouch model in mice was used to assess the immunomodulatory effect of M-Se@SiO_2 on inflammatory response and phenotypes of macrophages. Sterile air was injected subcutaneously to form an air pouch. As shown in Fig. 6A and 6B, hematoxylin and eosin (H&E) and Masson trichrome staining of air sac tissues from LPS-treated mice showed an increase in fibrous layer thickness and inflammatory cell infiltration. Fibrous layer thickness and inflammatory cell infiltration decreased in the LPS + M-Se@SiO_2 group compared with those in the LPS and LPS + Se@SiO_2 groups (Fig. 6C and 6D). The inflammatory exudates were used for cytokine detection by ELISA. The abundance of pro-inflammatory cytokines TNF-α and IL-6 was lower in the LPS + M-Se@SiO_2 group than in the LPS group, whereas that of the anti-inflammatory cytokines IL-4 and IL-10 was the highest in the LPS + M-Se@SiO_2 group, similar to the *in vitro* results (Fig. 6E). Immunofluorescence staining further demonstrated that the fibrous layer exhibited more CCR7-positive cells in the LPS group than in the control, LPS + Se@SiO_2, and LPS + M-Se@SiO_2 groups. In contrast, the number of ARG1-positive cells was higher in the LPS + M-Se@SiO_2 group, indicating that M-Se@SiO_2 induced M2-type polarization and an anti-inflammatory response (Fig. 6F). These findings indicate that M-Se@SiO_2 effectively inhibited LPS-induced inflammatory responses by regulating macrophage polarization.

After confirming that M-Se@SiO_2 has the potential to regulate macrophage polarization, we evaluated the potential of M-Se@SiO_2 to protect against LPS-induced inflammatory osteolysis using an *in vivo* cranial bone model in mice. After 14 days of surgery, microcomputed tomography analyses revealed increased cranial bone destruction and osteolysis in the LPS-treated group when compared with those in the control group (Fig. 7A and 7B). However, the treatment with M-Se@SiO_2 significantly inhibited osteolysis and

bone resorption. Furthermore, the quantitative analysis of morphometric parameters revealed that M-Se@SiO_2 treatment significantly inhibited the reduction in bone volume (BV/TV, ratio bone volume to tissue volume) and increased bone porosity after LPS-treatment (Fig. 7C, 7D, and 7E). Histological examination further confirmed the protective effects of M-Se@SiO_2 against LPS-induced osteolysis. H&E and Masson's trichrome staining revealed extensive bone resorption and inflammatory cell infiltration in the LPS group, whereas M-Se@SiO_2 treatment showed significantly less bone destruction and inflammation. Tartrate-resistant acid phosphatase (TRAP) staining showed that TRAP-positive cells were obviously induced by LPS, and the number of TRAP-positive cells decreased in the M-Se@SiO_2 treatment group. Collectively, our results suggest that treatment with M-Se@SiO_2 is protective against LPS-induced osteolytic bone loss *in vivo* (Fig. 8).

The *in vivo* biocompatibility was further evaluated in mice after 14 days of cranial surgery. H&E staining of the heart, liver, lung, spleen, and kidney confirmed nontoxicity (**Figure S1**). The strain shows excellent biocompatibility to nanoparticles, indicating the potential for its clinical application.

Conclusion

Our findings suggest that M-Se@SiO_2 has an immunomodulatory role in LPS-induced inflammation and bone remodeling. The results of our *in vitro* and *in vivo* experiments suggest that M-Se@SiO_2 inhibits the polarization of macrophages toward the M1 phenotype and reduces the release of pro-inflammatory factors while increasing the levels of anti-inflammatory, as well as osteogenic, factors to suppress inflammation and reduce osteolysis. At the molecular level, this effect might be mediated through the regulation of NF-κB and MAPK signaling pathways. In conclusion, M-Se@SiO_2 is a promising engineered nanoparticle for the treatment of osteolysis arising after arthroplasty, and it has potential for the further development of immunomodulatory nano-platforms.

Materials And Methods

Macrophage Membrane Derivation

Murine macrophage RAW264.7 cells, kindly provided by Stem Cell Bank (Chinese Academy of Sciences, China), were cultured in Dulbecco's modified Eagle's medium (Hyclone, USA) containing 10% fetal bovine serum (Gibco, Australia) and 1% penicillin/streptomycin (Gibco, USA) at 37 °C in 5% CO_2. The membrane was extracted from RAW264.7 cells using a membrane protein extraction kit (Beyotime, China). First, the cells were immersed for 15 min in ice-cold membrane protein extraction reagent; thereafter, cells were moderately disrupted using a Dounce homogenizer. Nuclei and a small number of unbroken cells were removed by low-speed centrifugation (700 × *g*, 10 min), and the supernatant was subjected to high-speed centrifugation (14000 × *g*, 30 min) to obtain the cell membrane precipitate. The membrane protein content was measured using a BCA kit (Beyotime). To obtain macrophage membrane vesicles, an ultrasound bath (42 kHz, 100 W) was used. Ultrasound was applied to cell membranes for 15 min,

followed by 11 extrusions using an Avanti mini extruder with 400 nm polycarbonate porous membranes (Avanti, Canada).[34]

M-Se@SiO_2 Preparation and Characterization:

Porous Se@SiO_2 nanospheres were synthesized according to our previous study [36]. First, $Cu_{2-x}Se$ nanocrystals were oxidized to form Se quantum dots. Solid Se@SiO_2 nanospheres were formed by coating silica onto Se quantum dots by orthosilicate hydrolysis in an alkaline environment. Next, the solid Se@SiO_2 nanospheres were coated with polyvinylpyrrolidone and treated with hot water to form porous structures. TEM (TF20; FEI, USA) and X-ray diffractometry (Rigaku, Japan) were used for nanoparticle detection and characterization. The collected macrophage membranes and porous Se@SiO_2 nanospheres were mixed at a 1:1 mass ratio of membrane proteins to nanoparticles using the ultrasound bath for 3 min. The membranes were then passed 11 times through 100 nm polycarbonate porous membranes using the Avestin mini extruder to obtain macrophage-membrane-coated porous Se@SiO_2 nanospheres (M-Se@SiO_2). M-Se@SiO_2 were detected by negative staining in TEM. Briefly, 3 μL of nanoparticle suspension (1 mg/mL) was deposited on a copper grid and subsequently stained with 1 wt% phosphotungstic acid. The samples were then observed using a Talos 120 kV Sphera microscope. Dynamic light scattering was used to measure the size and zeta potential of the nanoparticles. M-Se@SiO_2 at 1 mg/mL was mixed with 2× phosphate-buffered saline (PBS) at a 1:1 volume ratio, and its stability in PBS was assessed. The Se release from porous Se@SiO_2 nanospheres and M-Se@SiO2 was studied separately using a Leeman ICP-AES Prodigy instrument as previously described.[49]

LPS and Cytokine Neutralization

To evaluate the LPS- and cytokine binding ability of M-Se@SiO_2, M-Se@SiO_2 nanospheres (1 mg/mL) were mixed with PBS containing 10% fetal bovine serum (FBS) and fluorescein isothiocyanate (FITC)-LPS (Sigma, 100 ng/mL), TNF-α (85 pg/mL), or IL-6 (360 pg/mL) at 37 °C for 30 min. The samples were centrifuged at 16,000 × *g* for 15 min to remove the nanospheres. LPS remaining in the supernatant was measured as the fluorescence intensity, and cytokines in the supernatant were quantified by ELISA (Anogen, Canada).

Characterization of Membrane Proteins

Membrane proteins from macrophages were extracted using a membrane protein extraction kit (Beyotime) and the abundance of cell membrane surface proteins, including TLR4, TNFR1, and IL6-R, was detected by western blotting.

BMDM Cultures

The femurs of C57/BL6 mice were washed with α-modified Eagle's medium (α-MEM; Gibco, USA) to obtain bone marrow cells. The extracted cells were maintained in complete α-MEM containing 10% FBS (Gibco, Australia), 1% penicillin/streptomycin (Gibco, USA), and 40 ng/mL macrophage colony-

stimulating factor (Peprotech, USA) at 37 °C in 5% CO_2 for 7 d to obtain mouse BMDMs. The BMDMs were than seeded into cell culture plates and treated with LPS (Sigma, 100 ng/mL), with or without porous Se@SiO_2 nanospheres (Se@SiO_2 group; 10 μg/mL) or M-Se@SiO_2 (M-Se@SiO_2 group; 10 μg/mL).

Cell Biocompatibility Assay

Cell viability was analyzed using a Cell Counting Kit 8 (CCK-8; Dojindo, Japan). BMDMs were seeded in 24-well plates at a density of 5×10^5 per well, whereas BMSCs were plated at a density of 1×10^5 per well. After 24 h of incubation, the cells were cultured in medium containing 10% CCK-8 for 2 h at 37 °C. The absorbance was then read at 450 nm using a microplate reader (BioTek, USA)

Immunofluorescence Staining

Immunofluorescence staining of the M1-like macrophage marker CCR7 and M2-like macrophage marker ARG1 was performed to assess macrophage polarization. After 24 h of culture, cells were fixed in paraformaldehyde (4%), blocked with Blocking Buffer for Immunol Staining (Beyotime, China) for 15 min, and incubated with mouse anti-CCR7 (1:100, Abcam, USA) or rabbit anti-ARG1 (1:100, Abcam, USA) antibodies overnight at 4 °C. The next day, the cells were washed and incubated with donkey anti-mouse Alexa Fluor 594 (1:200, Abcam, USA) or donkey anti-rabbit Alexa Fluor 488 (1:200, Abcam, USA) for 1 h at room temperature protected from light. The cells were then washed with PBS and the nuclei were stained with 4′,6-dimidazole-2-phenylindole (DAPI) for 5 min. Images were taken using a DM8 microscope (Leica, USA).

Flow Cytometry

Flow cytometry was carried out to analyze the abundance of the M1 marker CCR7, M2 marker CD206, and general macrophage marker F4/80. After 24 h of culture, the cells were scraped, washed, blocked for 15 min with Blocking Buffer (Beyotime), and finally stained for 1 h with allophycocyanin (APC)-conjugated anti-CCR7 antibody (1:100, BioLegend, USA) or FITC-conjugated anti-CD206 antibody (1:100, BioLegend, USA). PE-conjugated anti-F4/80 (1:100, BioLegend, USA) was used to label all macrophages. The cells were analyzed using BD flow cytometry with the FlowJo software

Enzyme-Linked Immunosorbent Assays

After 24 h of incubation, the cell culture medium was collected and centrifuged. Cytokine levels (TNF-α, IL-4, IL-6, and IL-10) in the supernatant were determined using ELISA kits (Anogen, Canada) according to the manufacturer's instructions

Real-Time Polymerase Chain Reaction

After 24 h of incubation, the total RNA was extracted using an RNA extraction column kit (EZBioscience, USA) according to the manufacturer's instructions. Subsequently, complementary DNA was synthesized from 1 μg of total RNA using a cDNA synthesis kit (EZBioscience, USA). Quantitative RT-PCR was

performed using a SYBR Green Master mix (EZBioscience, USA) on LightCycler 480 (Roche, USA). The primers used are shown in **Table S1**.

Western Blotting

The cells were pretreated with Se@SiO_2 or M-Se@SiO_2 for 1 h, and then LPS was added (100 ng/mL). After 30 min, the cells were lysed with RIPA lysis buffer containing protease and phosphatase inhibitors (EpiZyme, China). The extracted total proteins were separated by sodium dodecyl sulfate-polyacrylamide gel electrophoresis and subsequently transferred onto polyvinylidene fluoride membranes. The membranes were blocked in blocking solution (Beyotime) for 15 min, washed, and incubated with primary antibodies overnight at 4 °C. p38/p-p38, extracellular signal-regulated kinase (ERK)/p-ERK, and p65/p-p65 antibodies (1:1000, Cell Signaling, USA) were used for the experiments. After washing, the membranes were incubated with goat anti-rabbit IgG-horseradish peroxidase (1:1000, Cell Signaling, USA) for 1 h at room temperature. Blots were developed with enhanced chemiluminescent reagent (Millipore, USA) and Tanon Imaging System (Tanon, China) for chemiluminescent detection. Relative band intensities were quantified using ImageJ software, and all results were normalized to β-actin expression.

BMSC Cultures and Conditioned Medium Preparation

Primary mouse BMSCs were isolated as previously described[4] and cultured in α-MEM containing 10% FBS and 1% penicillin/streptomycin. After culturing BMDMs for 24 h, media from the control, LPS, LPS+Se@SiO_2 and LPS+M-Se@SiO_2 group cultures were collected and centrifuged; the resulting supernatant was then mixed with osteogenic induction medium (Cygen, China) at a ratio of 1:2 to obtain the conditioned medium. Next, BMSCs were seeded into 24-well plates at a density of 2.5×10^4 cells per well. Following cell adherence, the culture medium was replaced with conditioned medium, which was subsequently changed every two days

Alkaline Phosphatase (ALP) and Alizarin Red (ARS) Staining

BMSCs were fixed using 4% paraformaldehyde and stained with ALP (Beyotime, China) or ARS (Cytogen, China) dyes after 14 d of culture. ALP was quantified using an ALP assay kit (Beyotime, China) according to the manufacturer's instructions. Quantitative analysis of ARS staining was performed by adding 10% acetylchlorinated pyridine to release ARS after ARS staining and subsequently by measuring the optical density at 600 nm.

Analysis of Gene Expression in BMSCs Exposed to BMDM-Conditioned Medium

After 2 weeks of incubation, the expression of the osteogenesis-related genes of bone morphogenetic protein-2 (*BMP-2*), osteocalcin (*OCN*), and osteopontin (*OPN*) was analyzed by RT-PCR. The primers used are shown in Table S1

In Vivo Air Pouch Model in Mice

The animal experiments were approved by the Animal Care Committee of Shanghai Jiao Tong University Affiliated Sixth People's Hospital. C57BL/6 mice were used in the experiments as described previously.[5] After mild anesthesia of the mice using pentobarbital, 5 mL of sterile air was injected subcutaneously. Four days after air pouch formation, 0.5 mL PBS or 0.5 mL PBS with 1 μg/mL LPS was injected with or without porous Se@SiO_2 or M-Se@SiO_2. Four days after injection, the mice were sacrificed, and exudates obtained by washing the air pouches with 2 mL PBS were centrifuged and stored at −80 °C for ELISA. Finally, the air pouch tissue was collected and fixed with 4% paraformaldehyde. Tissue sections were subjected to hematoxylin and eosin (H&E) or Masson trichrome staining to assess inflammation, immune cell infiltration, and membrane thickness. Immunofluorescence staining was used to detect CCR7- and ARG1-positive cells in the air pouch tissue. Images were captured using a DM6 microscope (Leica, USA) and analyzed using the ImageJ software.

In Vivo Calvarial Osteolysis Model in Mice

Mice were anesthetized with intraperitoneal pentobarbital injections. A 1-cm long incision was made in the middle of the cranium, and the cranial periosteum was separated from the calvarium. Next, 50 μL of LPS (1 mg/mL) was embedded under the periosteum around the sagittal midline suture of the calvaria. In the experimental groups, PBS, porous Se@SiO_2, or M-Se@SiO_2 were injected intraperitoneally at a dose of 0.5 mg/kg every 3 d. The animals were sacrificed 14 d after surgery. The cranial bones were carefully harvested, fixed in 4% paraformaldehyde, and stored in 70% ethanol until they were imaged with a micro-CT scanner (Bruker micro-CT) at a resolution of 18 mm. Bone volume to tissue volume ratio (BV/TV), total porosity, and the number of pores were measured and analyzed using CT Analyser Software (Bruker) as previously described.[50] Before to paraffin embedding, bones were decalcified in 14% EDTA, pH 7.4 for 2 weeks. Thereafter, H&E Masson trichrome and tartrate-resistant acid phosphatase (TRAP) staining was performed. The stained sections were imaged using a DM6 microscope (Leica, USA). In addition, the heart, kidney, liver, spleen and lungs of mice were collected and fixed to assess biosafety aspects of the administered nanoparticles in major organs. The sections of major organs were paraffin-embedded, cut, and stained with H&E.

Statistical analysis

Data are presented as mean ± standard deviation and were analyzed with SPSS v. 18.0 software (SPSS Inc., Chicago, IL, USA). Statistical significance among groups was evaluated using the one-way analysis of variance and the *t*-test. Results with $p < 0.05$ were considered statistically significant.

Abbreviations

Se@SiO_2: SiO_2-coated ultrasmall Se particles; M-Se@SiO_2: macrophage-membrane-coated porous Se@SiO_2 nanospheres; LPS: lipopolysaccharide; ERK: extracellular signal-regulated kinase; IL: interleukin; TNF-α: tumor necrosis factor-alpha; TLR4: toll-like receptor 4; MAPK: p38 mitogen-activated protein kinase; TEM: transmission electron microscopy; XRD: X-ray diffractometry; DLS: dynamic light scattering;

CCK-8: Cell Counting Kit 8; BMDM: bone marrow-derived macrophage; BMSC:bone mesenchymal stem cell; iNOS: inducible nitric oxide synthase; CCR7: C-C chemokine receptor type 7; ARG1: arginase 1; RT-PCR: real-time polymerase chain reaction; BMP2: bone morphogenetic protein-2; ELISA: enzyme-linked immunosorbent assay; NF-κB: nuclear factor-κB; JNK: c-Jun N-terminal kinase; ALP: alkaline phosphatase; ARS: alizarin red; OCN: osteocalcin; OPN: osteopontin; BV/TV: ratio bone volume to tissue volume; TRAP: tartrate-resistant acid phosphatase; PBS: phosphate-buffered saline; α-MEM: α-modified Eagle's medium; FBS: fetal bovine serum; DAPI: 4′,6-dimidazole-2-phenylindole; FITC: fluorescein isothiocyanate; H&E: hematoxylin and eosin.

Declarations

Authors' contributions

CD, CY and TC carried out experiments and wrote the paper. JX-W, XJ-L and XL-Z designed the study. XY-W contributed to sample preparation. QJ-W, RK-H, SS, KC-Z and DD-X gave guidance and assistance on the biology knowledge and experiments. All authors approved the final manuscript.

Acknowledgements

This work was supported by the National Natural Science Foundation of China (Grant No. 81772309, 81974324, and 81802181) and the Shanghai Pujiang Talent Program (18PJD035).

Competing interests

The authors declare that they have no competing interests.

Availability of data and materials

All data of this study are included in this article

Consent for publication

All authors read and approved the final manuscript for publication

Ethics approval and consent to participate

The animal experiments were approved by the Animal Care Committee of Shanghai Jiao Tong University Affiliated Sixth People's Hospital.

Funding

This work was financially supported by the National Natural Science Foundation of China (Grant No. 81772309, 81974324, and 81802181) and the Shanghai Pujiang Talent Program (18PJD035).

References

1. Rao AJ, Gibon E, Ma T, Yao Z, Smith RL, Goodman SB. Revision joint replacement, wear particles, and macrophage polarization. Acta Biomater. 2012;8:2815–23.
2. Tande AJ, Patel R. Prosthetic joint infection. Clin Microbiol Rev. 2014;27:302–45.
3. Bi Y, Seabold JM, Kaar SG, Ragab AA, Goldberg VM, Anderson JM, Greenfield EM. Adherent endotoxin on orthopedic wear particles stimulates cytokine production and osteoclast differentiation. Journal of bone mineral research: the official journal of the American Society for Bone Mineral Research. 2001;16:2082–91.
4. Purdue PE, Koulouvaris P, Potter HG, Nestor BJ, Sculco TP. The cellular and molecular biology of periprosthetic osteolysis. Clin Orthop Relat Res. 2007;454:251–61.
5. Yang C, Wang W, Zhu K, Liu W, Luo Y, Yuan X, Wang J, Cheng T, Zhang X. Lithium chloride with immunomodulatory function for regulating titanium nanoparticle-stimulated inflammatory response and accelerating osteogenesis through suppression of MAPK signaling pathway. Int J Nanomedicine. 2019;14:7475–88.
6. Murray PJ. Macrophage Polarization. Annu Rev Physiol. 2017;79:541–66.
7. Zhu K, Yang C, Dai H, Li J, Liu W, Luo Y, Zhang X, Wang Q. Crocin inhibits titanium particle-induced inflammation and promotes osteogenesis by regulating macrophage polarization. Int Immunopharmacol. 2019;76:105865.
8. Di Benedetto P, Ruscitti P, Vadasz Z, Toubi E, Giacomelli R. Macrophages with regulatory functions, a possible new therapeutic perspective in autoimmune diseases. Autoimmun Rev. 2019;18:102369.
9. Shapouri-Moghaddam A, Mohammadian S, Vazini H, Taghadosi M, Esmaeili SA, Mardani F, Seifi B, Mohammadi A, Afshari JT, Sahebkar A. Macrophage plasticity, polarization, and function in health and disease. J Cell Physiol. 2018;233:6425–40.
10. Liu W, Li J, Cheng M, Wang Q, Yeung KWK, Chu PK, Zhang X. Zinc-Modified Sulfonated Polyetheretherketone Surface with Immunomodulatory Function for Guiding Cell Fate and Bone Regeneration. Adv Sci (Weinh). 2018;5:1800749.
11. Yang C, Ouyang L, Wang W, Chen B, Liu W, Yuan X, Luo Y, Cheng T, Yeung KWK, Liu X, Zhang X. Sodium butyrate-modified sulfonated polyetheretherketone modulates macrophage behavior and shows enhanced antibacterial and osteogenic functions during implant-associated infections. J Mater Chem B. 2019;7:5541–53.
12. Niu Y, Wang Z, Shi Y, Dong L, Wang C. Modulating macrophage activities to promote endogenous bone regeneration: Biological mechanisms and engineering approaches. Bioact Mater. 2021;6:244–61.
13. Rayman MP. Selenium and human health. The Lancet. 2012;379:1256–68.
14. Avery JC, Hoffmann PR: Selenium, Selenoproteins, and Immunity. *Nutrients* 2018, 10.
15. Huang Z, Rose AH, Hoffmann PR. The role of selenium in inflammation and immunity: from molecular mechanisms to therapeutic opportunities. Antioxid Redox Signal. 2012;16:705–43.

16. Yun CH, Yang JS, Kang SS, Yang Y, Cho JH, Son CG, Han SH. NF-kappaB signaling pathway, not IFN-beta/STAT1, is responsible for the selenium suppression of LPS-induced nitric oxide production. Int Immunopharmacol. 2007;7:1192–8.
17. Nelson SM, Lei X, Prabhu KS. Selenium levels affect the IL-4-induced expression of alternative activation markers in murine macrophages. J Nutr. 2011;141:1754–61.
18. Lv Q, Liang X, Nong K, Gong Z, Qin T, Qin X, Wang D, Zhu Y. Advances in Research on the Toxicological Effects of Selenium. Bull Environ Contam Toxicol. 2021;106:715–26.
19. Liu X, Deng G, Wang Y, Wang Q, Gao Z, Sun Y, Zhang W, Lu J, Hu J. A novel and facile synthesis of porous SiO2-coated ultrasmall Se particles as a drug delivery nanoplatform for efficient synergistic treatment of cancer cells. Nanoscale. 2016;8:8536–41.
20. Akira S, Takeda K, Kaisho T. Toll-like receptors: critical proteins linking innate and acquired immunity. Nature immunology. 2001;2:675–80.
21. Hotokezaka H, Sakai E, Ohara N, Hotokezaka Y, Gonzales C, Matsuo K, Fujimura Y, Yoshida N, Nakayama K. Molecular analysis of RANKL-independent cell fusion of osteoclast-like cells induced by TNF-alpha, lipopolysaccharide, or peptidoglycan. J Cell Biochem. 2007;101:122–34.
22. Liu J, Tang J, Zuo Y, Yu Y, Luo P, Yao X, Dong Y, Wang P, Liu L, Zhou H. Stauntoside B inhibits macrophage activation by inhibiting NF-kappaB and ERK MAPK signalling. Pharmacol Res. 2016;111:303–15.
23. Lin A, Liu Y, Zhu X, Chen X, Liu J, Zhou Y, Qin X, Liu J. Bacteria-Responsive Biomimetic Selenium Nanosystem for Multidrug-Resistant Bacterial Infection Detection and Inhibition. ACS Nano. 2019;13:13965–84.
24. Wang D, Dong H, Li M, Cao Y, Yang F, Zhang K, Dai W, Wang C, Zhang X. Erythrocyte-Cancer Hybrid Membrane Camouflaged Hollow Copper Sulfide Nanoparticles for Prolonged Circulation Life and Homotypic-Targeting Photothermal/Chemotherapy of Melanoma. ACS Nano. 2018;12:5241–52.
25. Xiong K, Wei W, Jin Y, Wang S, Zhao D, Wang S, Gao X, Qiao C, Yue H, Ma G, Xie HY. Biomimetic Immuno-Magnetosomes for High-Performance Enrichment of Circulating Tumor Cells. Adv Mater. 2016;28:7929–35.
26. Hu CM, Fang RH, Copp J, Luk BT, Zhang L. A biomimetic nanosponge that absorbs pore-forming toxins. Nat Nanotechnol. 2013;8:336–40.
27. Piao J-G, Wang L, Gao F, You Y-Z, Xiong Y, Yang L. Erythrocyte membrane is an alternative coating to polyethylene glycol for prolonging the circulation lifetime of gold nanocages for photothermal therapy. ACS Nano. 2014;8:10414–25.
28. Zhao Q, Sun X, Wu B, Shang Y, Huang X, Dong H, Liu H, Chen W, Gui R, Li J. Construction of homologous cancer cell membrane camouflage in a nano-drug delivery system for the treatment of lymphoma. J Nanobiotechnology. 2021;19:8.
29. Fang RH, Jiang Y, Fang JC, Zhang L. Cell membrane-derived nanomaterials for biomedical applications. Biomaterials. 2017;128:69–83.

30. Ai X, Hu M, Wang Z, Zhang W, Li J, Yang H, Lin J, Xing B. Recent Advances of Membrane-Cloaked Nanoplatforms for Biomedical Applications. Bioconjug Chem. 2018;29:838–51.
31. Gong H, Zhang Q, Komarla A, Wang S, Duan Y, Zhou Z, Chen F, Fang RH, Xu S, Gao W, Zhang L. Nanomaterial Biointerfacing via Mitochondrial Membrane Coating for Targeted Detoxification and Molecular Detection. Nano Lett. 2021;21:2603–9.
32. Liao Y, Zhang Y, Blum NT, Lin J, Huang P. Biomimetic hybrid membrane-based nanoplatforms: synthesis, properties and biomedical applications. Nanoscale Horiz. 2020;5:1293–302.
33. Thamphiwatana S, Angsantikul P, Escajadillo T, Zhang Q, Olson J, Luk BT, Zhang S, Fang RH, Gao W, Nizet V, Zhang L. Macrophage-like nanoparticles concurrently absorbing endotoxins and proinflammatory cytokines for sepsis management. Proc Natl Acad Sci U S A. 2017;114:11488–93.
34. Wang Y, Zhang K, Li T, Maruf A, Qin X, Luo L, Zhong Y, Qiu J, McGinty S, Pontrelli G, et al. Macrophage membrane functionalized biomimetic nanoparticles for targeted anti-atherosclerosis applications. Theranostics. 2021;11:164–80.
35. Yin C, Zhao Q, Li W, Zhao Z, Wang J, Deng T, Zhang P, Shen K, Li Z, Zhang Y. Biomimetic anti-inflammatory nano-capsule serves as a cytokine blocker and M2 polarization inducer for bone tissue repair. Acta Biomater. 2020;102:416–26.
36. Zheng N, Wang Q, Li C, Wang X, Liu X, Wang X, Deng G, Wang J, Zhao L, Lu J. Responsive Degradable Theranostic Agents Enable Controlled Selenium Delivery to Enhance Photothermal Radiotherapy and Reduce Side Effects. Adv Healthc Mater. 2021;10:e2002024.
37. Zhang Q, Dehaini D, Zhang Y, Zhou J, Chen X, Zhang L, Fang RH, Gao W, Zhang L. Neutrophil membrane-coated nanoparticles inhibit synovial inflammation and alleviate joint damage in inflammatory arthritis. Nat Nanotechnol. 2018;13:1182–90.
38. Gao W, Fang RH, Thamphiwatana S, Luk BT, Li J, Angsantikul P, Zhang Q, Hu CM, Zhang L. Modulating antibacterial immunity via bacterial membrane-coated nanoparticles. Nano Lett. 2015;15:1403–9.
39. Hu CM, Fang RH, Wang KC, Luk BT, Thamphiwatana S, Dehaini D, Nguyen P, Angsantikul P, Wen CH, Kroll AV, et al. Nanoparticle biointerfacing by platelet membrane cloaking. Nature. 2015;526:118–21.
40. Li C, Wang Q, Gu X, Kang Y, Zhang Y, Hu Y, Li T, Jin H, Deng G, Wang Q. Porous Se@SiO2 nanocomposite promotes migration and osteogenic differentiation of rat bone marrow mesenchymal stem cell to accelerate bone fracture healing in a rat model. Int J Nanomedicine. 2019;14:3845–60.
41. Zheng Z, Deng G, Qi C, Xu Y, Liu X, Zhao Z, Zhang Z, Chu Y, Wu H, Liu J. Porous Se@SiO2 nanospheres attenuate ischemia/reperfusion (I/R)-induced acute kidney injury (AKI) and inflammation by antioxidative stress. Int J Nanomedicine. 2019;14:215–29.
42. Qin L, Zhang Y, Wan C, Wang Z, Cong Y, Li S. MiR-196-5p involvement in selenium deficiency-induced immune damage via targeting of NFkappaBIA in the chicken trachea. Metallomics. 2020;12:1679–92.

43. Yang BY, Deng GY, Zhao RZ, Dai CY, Jiang CY, Wang XJ, Jing YF, Liu XJ, Xia SJ, Han BM. Porous Se@SiO2 nanosphere-coated catheter accelerates prostatic urethra wound healing by modulating macrophage polarization through reactive oxygen species-NF-kappaB pathway inhibition. Acta Biomater. 2019;88:392–405.
44. Zhu X, Gao J, Ng PY, Qin A, Steer JH, Pavlos NJ, Zheng MH, Dong Y, Cheng TS. Alexidine Dihydrochloride Attenuates Osteoclast Formation and Bone Resorption and Protects Against LPS-Induced Osteolysis. J Bone Miner Res. 2016;31:560–72.
45. Guo G, Gong T, Shen H, Wang Q, Jiang F, Tang J, Jiang X, Wang J, Zhang X, Bu W. Self-Amplification Immunomodulatory Strategy for Tissue Regeneration in Diabetes Based on Cytokine-ZIFs System. *Advanced Functional Materials* 2021.
46. Li X, Zou Y, Fu YY, Xing J, Wang KY, Wan PZ, Wang M, Zhai XY. Ibudilast Attenuates Folic Acid-Induced Acute Kidney Injury by Blocking Pyroptosis Through TLR4-Mediated NF-kappaB and MAPK Signaling Pathways. Front Pharmacol. 2021;12:650283.
47. Seno M, Liu C-P, Zhang X, Tan Q-L, Xu W-X, Zhou C-Y, Luo M, Li X, Huang R-Y, Zeng X. NF-κB pathways are involved in M1 polarization of RAW 264.7 macrophage by polyporus polysaccharide in the tumor microenvironment. *Plos One* 2017, 12.
48. Bi CL, Wang H, Wang YJ, Sun J, Dong JS, Meng X, Li JJ. Selenium inhibits Staphylococcus aureus-induced inflammation by suppressing the activation of the NF-kappaB and MAPK signalling pathways in RAW264.7 macrophages. Eur J Pharmacol. 2016;780:159–65.
49. Wang Y, Liu X, Deng G, Sun J, Yuan H, Li Q, Wang Q, Lu J. Se@SiO2–FA–CuS nanocomposites for targeted delivery of DOX and nano selenium in synergistic combination of chemo-photothermal therapy. Nanoscale. 2018;10:2866–75.
50. Yang C, Li J, Zhu K, Yuan X, Cheng T, Qian Y, Zhang X. Puerarin Exerts Protective Effects on Wear Particle-Induced Inflammatory Osteolysis. Front Pharmacol. 2019;10:1113.

Figures

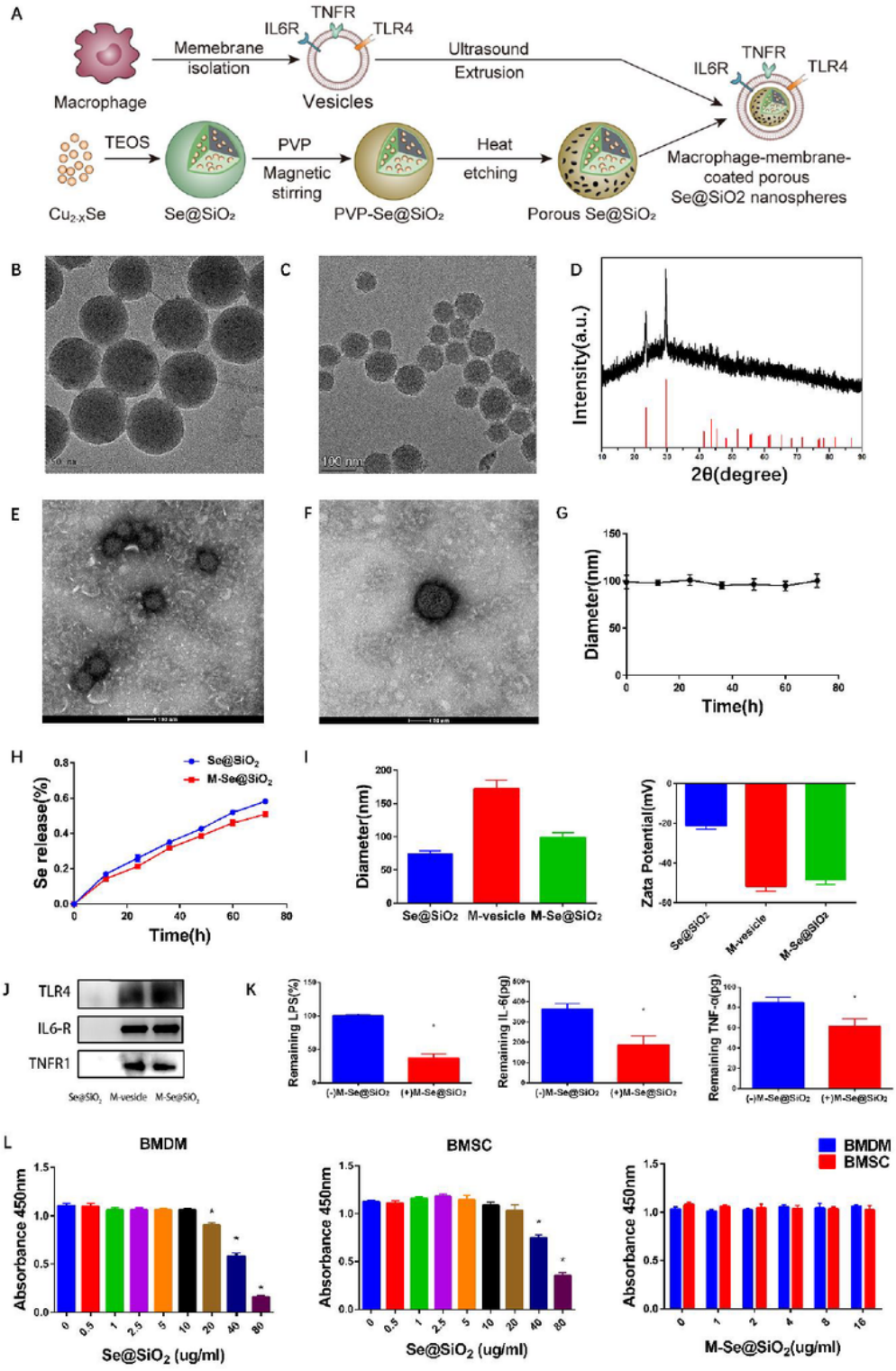

Figure 1

Characterization of the macrophage-membrane-coated porous Se@SiO2 nanospheres. (A) Schematic diagram of M-Se@SiO2 synthesis. TEM images of (B) Se@SiO2, (C) porous Se@SiO2, and (E, F) M-Se@SiO2. (D) X-ray diffractometry pattern of Se@SiO2 nanospheres and the standard Se hexagonal phase (JCPDS card No. 06-0362). (G) Hydrodynamic sizes of M-Se@SiO2 in PBS over 72 h. (H) Se release from M-Se@SiO2 and porous Se@SiO2 in PBS at 37 °C and pH 7.4 over 72 h. (I) Size and zeta

potential of porous Se@SiO2, M-vesicle, and M-Se@SiO2. (J) Western blots of TLR4, TNFR1, and IL6-R in porous Se@SiO2, M-vesicle, and M-Se@SiO2. (K) Removal of LPS and pro-inflammatory cytokines IL-6 and TNF-α by M-Se@SiO2. (L) Cell biocompatibility was evaluated by CCK-8 after 1 d of culture (*p < 0.05 compared with the Control).

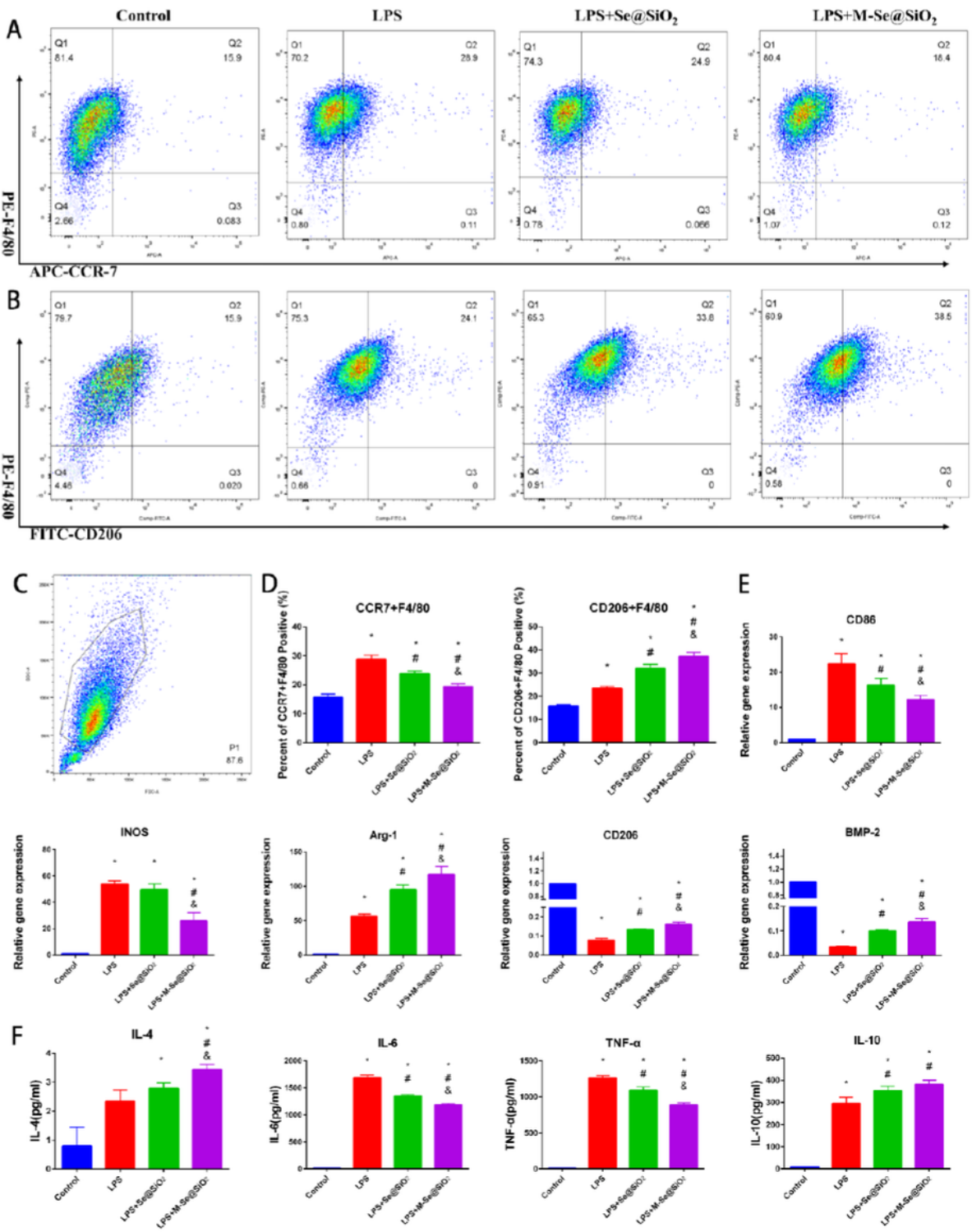

Figure 2

In vitro polarization of macrophages. (A, B) Representative dot images of flow cytometry results after 24 h of culture of bone marrow-derived macrophages. Percentages of CCR7-, CD206-, and F4/80-positive cells. (C) Representative forward scatter (FSC) and side scatter (SSC) gates. (D) Proportion of CCR7+F4/80- and CD206+F4/80-positive cells. (E) RT-PCR results of CD86, iNOS, ARG1, CD206, and BMP-2 expression. (F) ELISA results of IL-4, IL-6, TNF-α, and IL-10 (*, #, and & represent $p < 0.05$ compared with the Control, LPS, and LPS+Se@SiO2, respectively).

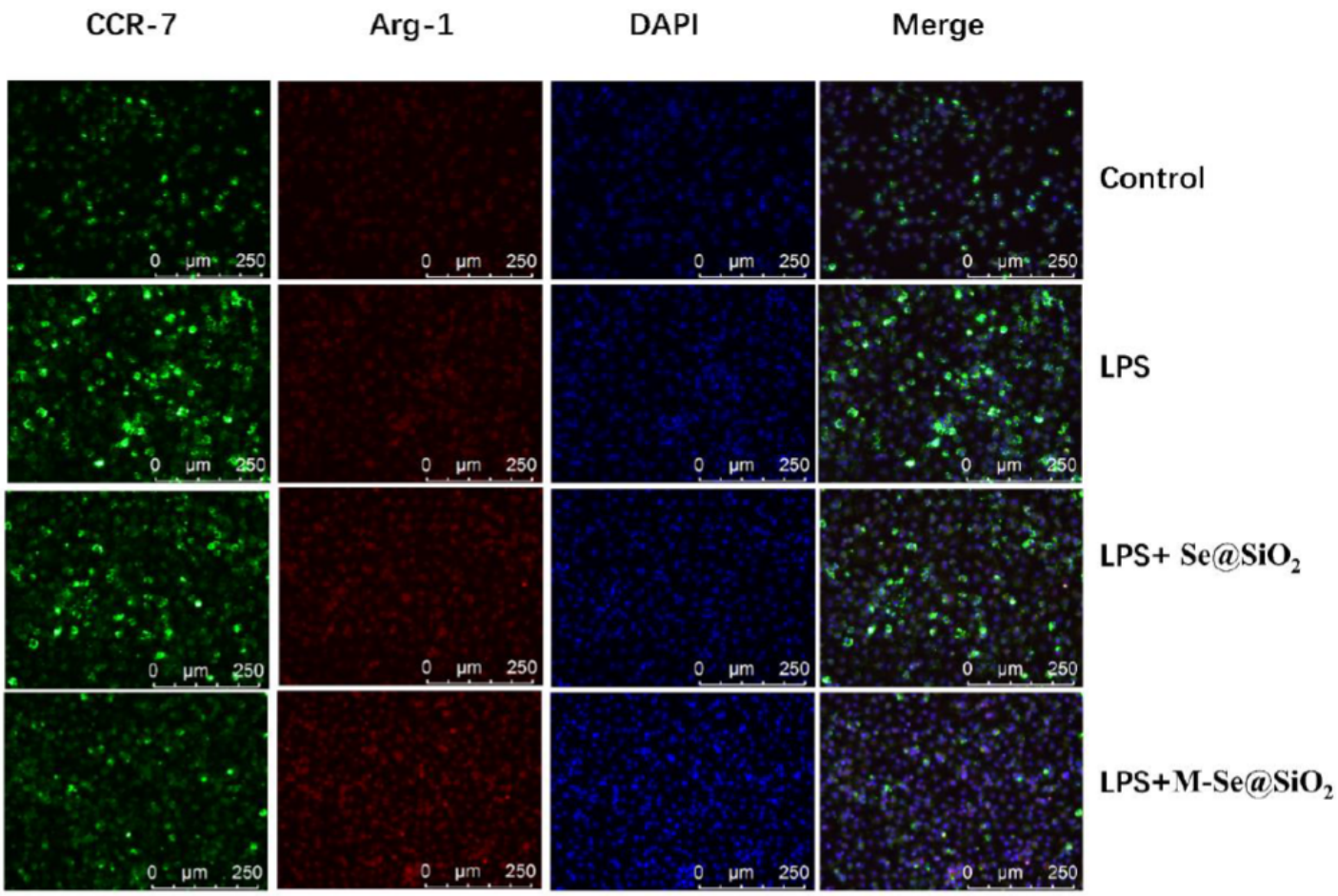

Figure 3

Immunofluorescence staining of BMDMs. CCR7 (green), ARG1 (red), and DAPI (blue; nuclei).

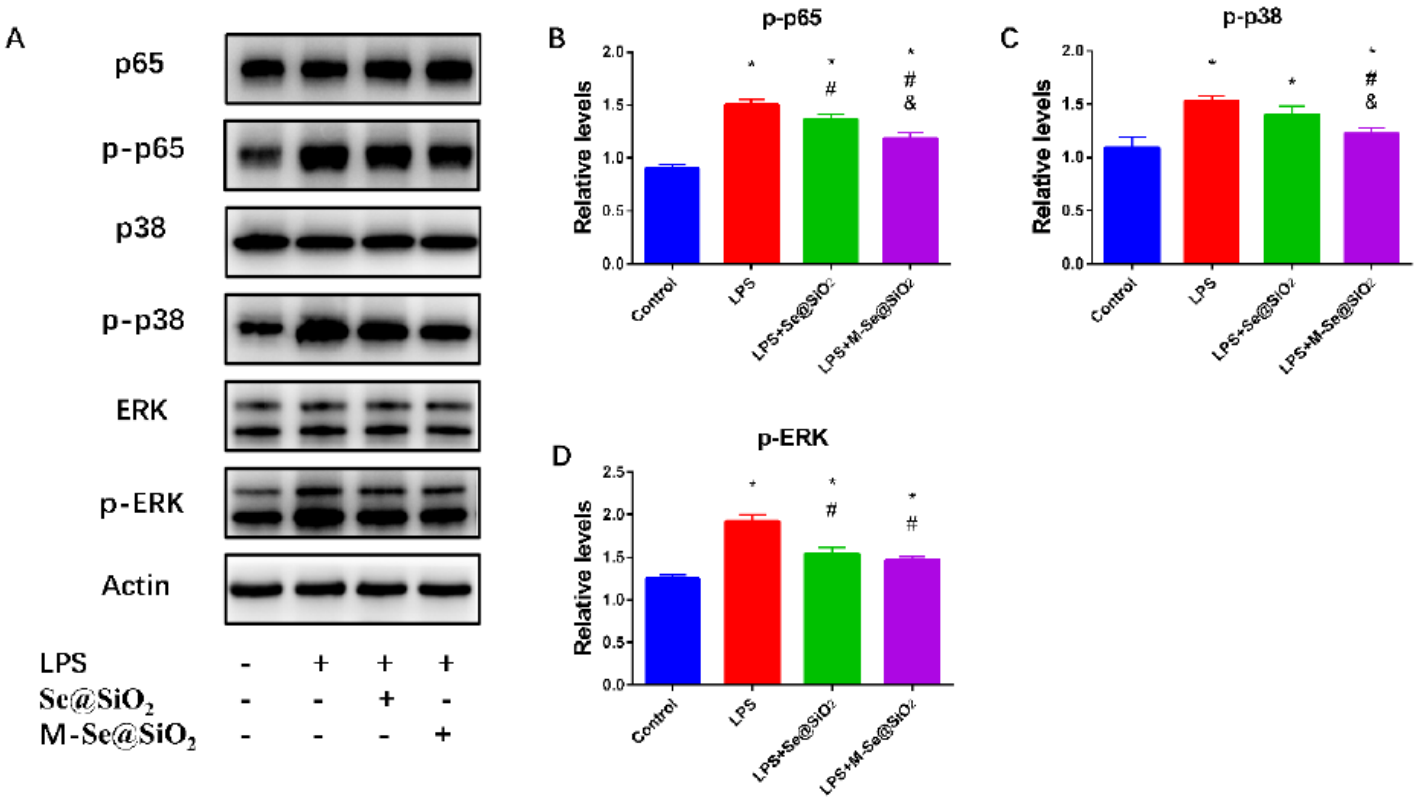

Figure 4

M-Se@SiO2 attenuates LPS-induced phosphorylation of p65, ERK, and p38 in BMDM cells. (A) Western blots of macrophages treated with PBS (Control), LPS, LPS+Se@SiO2, or LPS+M-Se@SiO2. (B–D) Relative quantification of signal intensity of western blot bands shown in (A) (*, #, and & represent $p < 0.05$ compared with the Control, LPS, and LPS+Se@SiO2, respectively).

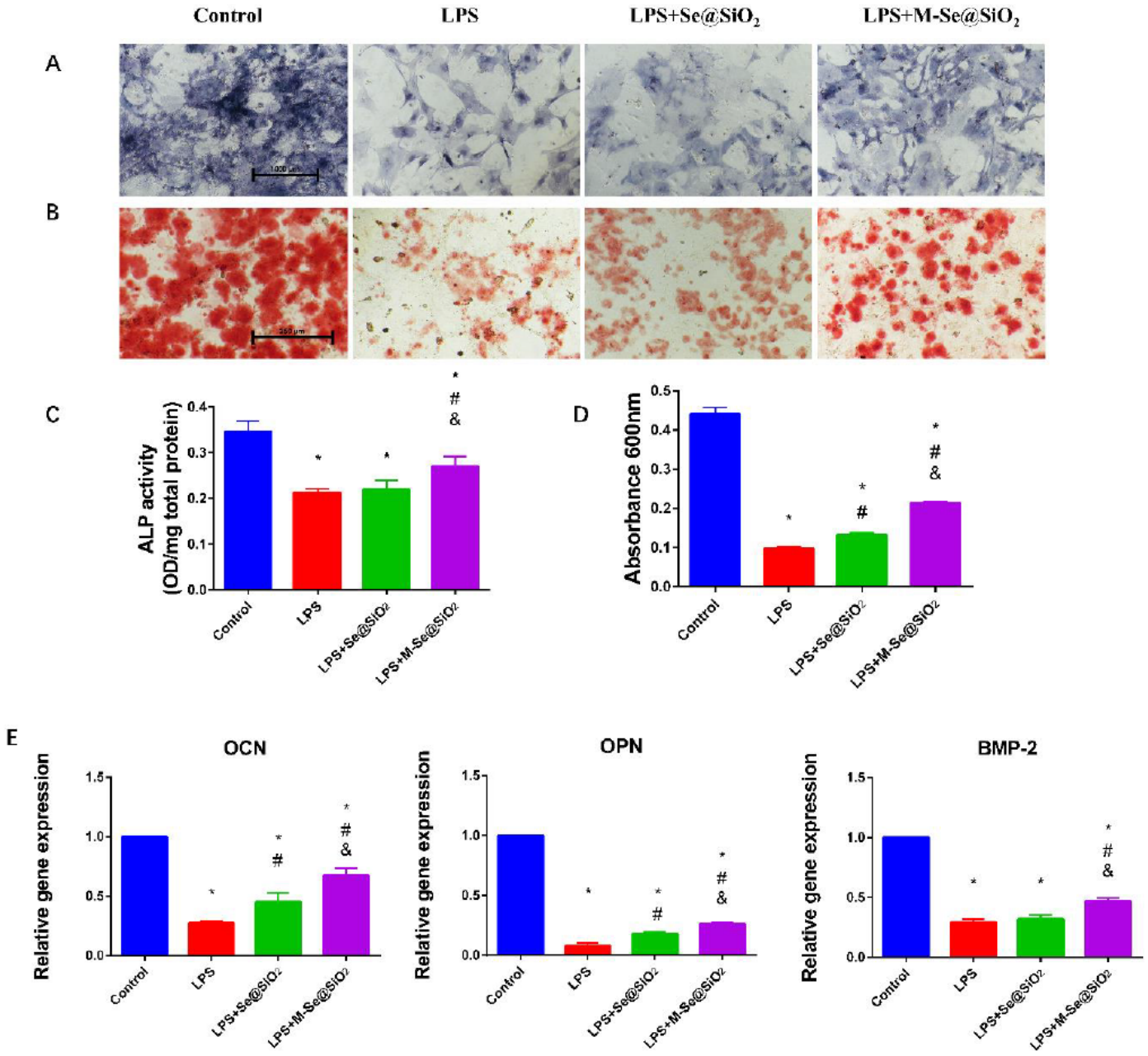

Figure 5

Osteogenic differentiation by macrophage-conditioned medium. (A) ALP and (B) ARS staining of BMSCs cultured in conditioned medium for 14 d. (C) ALP activity of BMSCs cultured in conditioned medium. (D) Quantitative analysis of ARS staining. (E) Osteogenesis-related gene expression of BMSCs cultured in conditioned medium (*, #, and & represent $p < 0.05$ compared with the Control, LPS, and LPS+Se@SiO2, respectively).

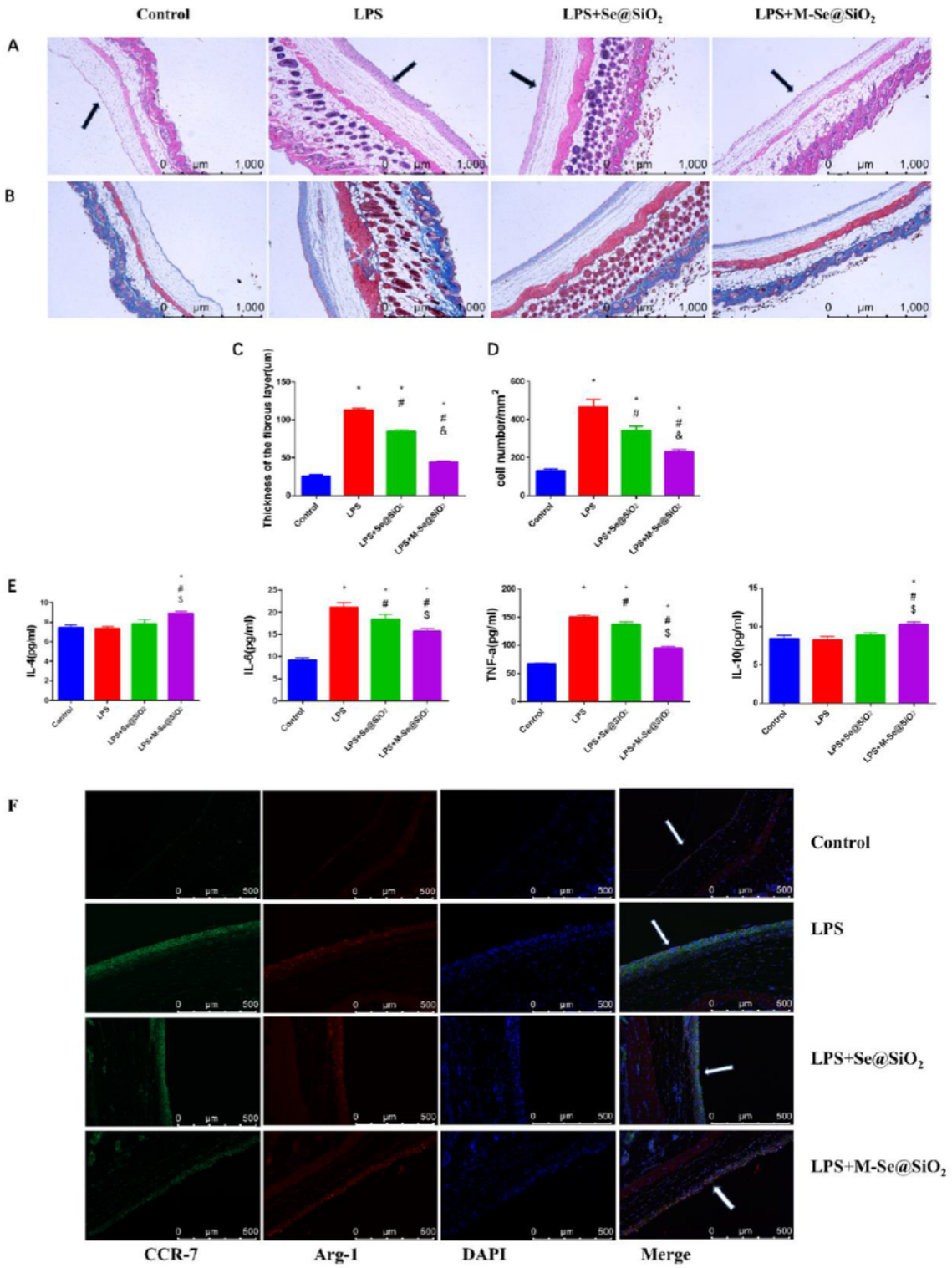

Figure 6

Staining of air pouch tissues on day 4. (A) H&E and (B) Masson trichrome staining of skin tissue from air pouches. Arrows point to the fibrous layer. (C) Thickness of the fibrous layer. (D) Numbers of infiltrating cells. (E) Cytokines in air pouch exudates evaluated by ELISA. (F) Immunofluorescence staining of skin tissue from air pouches. CCR7 (green), ARG1 (red), and DAPI (blue; nuclei). Arrows point to the fibrous layer (*, #, and & represent $p < 0.05$ compared with the Control, LPS, and LPS+Se@SiO2, respectively).

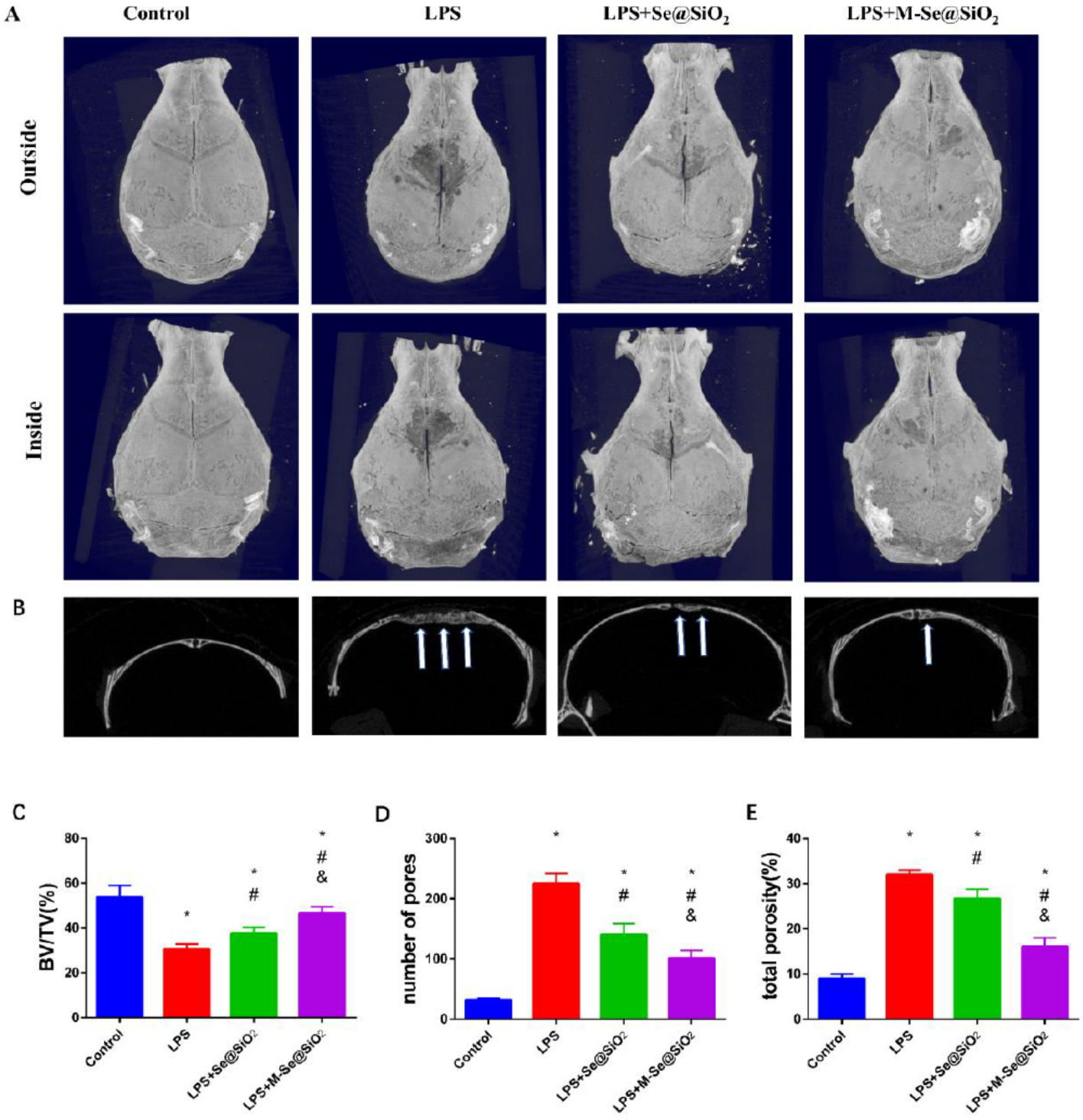

Figure 7

M-Se@SiO2 attenuates LPS-induced osteolysis in vivo. Representative micro-CT (A) 3D- and (B) 2D-reconstructed images of the calvaria in each group. White arrows indicate osteolysis. (C) BV/TV, (D) number of pores, and (E) total porosity in each group were measured using micro-CT analyzer software (*, #, and & represent $p < 0.05$ compared with the Control, LPS, and LPS+Se@SiO2, respectively).

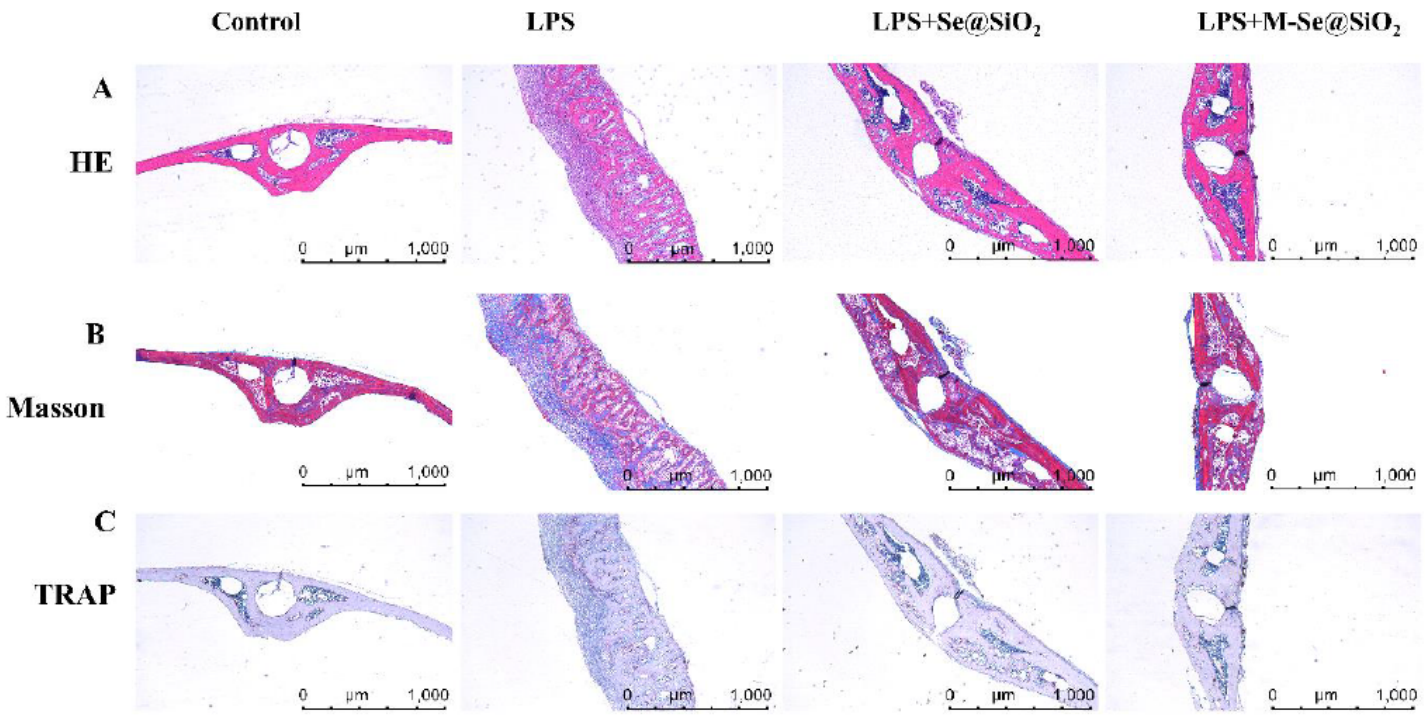

Figure 8

Histological images of (A) H&E-stained, (B) Masson trichrome-, and (C) TRAP-stained calvarium sections in each experimental group.

Supplementary Files

This is a list of supplementary files associated with this preprint. Click to download.

- SI.docx
- Scheme1.png